Heliyon 8 (2022) e10908

Contents lists available at ScienceDirect

Heliyon

journal homepage: www.cell.com/heliyon

Research article

Removal of reactive violet 5 azodye (V5R) using bamboo, and calabash biochar

Samuel Kofi Tulashie [a,*], Francis Kotoka [a], Bennett Nana Botchway [a], Kofi Adu [b]

[a] University of Cape Coast, College of Agriculture and Natural Sciences, School of Physical Sciences, Department of Chemistry, Industrial Chemistry Unit, Cape Coast, Ghana

[b] University of Cape Coast, College of Agriculture and Natural Sciences, School of Physical Sciences, Department of Physics, Industrial Chemistry Unit, Cape Coast, Ghana

ARTICLE INFO

Keywords:
Adsorption isotherm
Kinetics
Adsorptive capacity

ABSTRACT

We assess the adsorption capacity of bamboo and calabash biochar (BB and CB). Using 10–50 mg/L Reactive Violet 5 Azo dye (V5R) adsorbate, the kinetics, and adsorption isotherms are investigated. We pyrolyzed the bamboo, and calabash biomass at 500 °C, washed, and oven dried at 120 °C for 48 h. The Brunauer–Emmett–-Teller (BET) method indicates that the BB and CB average pore diameters are 21.1 nm and 26.5 nm, with specific surface areas of 174.67 m^2/g and 44.78 m^2/g, respectively. The SEM reveals a larger granular shape of the CB having pinholes on the surface, but the BB exhibited interconnected structures like a mesh. The FTIR shows C=C, C=O, O–H, and C–O–C as the predominant functional groups on both BB and CB. The adsorption of V5R on BB and CB follows pseudo-second-order kinetics and favors Langmuir isotherm with maximum adsorption capacities of 5.106 mg/g, and 0.010 mg/g, respectively. The BB adsorbs 70.9–96% V5R, whilst CB adsorbs 0.1–0.2 % only. The results suggest that bamboo biochar has the potential to eliminate 70.9–96% of 10–50 mg/L V5R from an aqueous solution, hence suitable for removing V5R. In this study, we have also presented a prototype expected to eliminate 91.6%–99.8% of the V5R from an aqueous solution.

1. Introduction

Wrong disposal of industrial effluent endangers human life and the environment [1]. Textile industries are one of the major contributors to the degradation of surface and groundwater, hence, categorized among the most polluting industries [2]. They use a large volume of water, and their waste contains several chemicals and coloring compounds, requiring appropriate treatment before being discharged into any water bodies [3]. For example, azo dyes contribute 70% of the total dye production [4], and by estimation, the textile industries apply 80% of azo dyes [4], during which 10–15% of these dyes escape to the environment [5], inducing color change, rise in pH, increase chemical oxygen demands (COD), and biological oxygen demands (BOD) [6, 7, 8]. Dyes can have adverse effects on humans, such as skin irritation and cancer [9], and also affect photosynthetic activities [10] For instance, results from humans and laboratory animals indicate that benzidine-structured azo dyes have a carcinogenic impact and induces tumor in the human urinary bladder and animals, respectively [4]. Therefore, in recent years, interest in the control of water pollution has risen as a key concern worldwide. Human eyes can detect reactive dye at approximately 0.005 mg/L in the waste flow; therefore, wastewater exceeding limits could not be allowed for aesthetic reasons [11].

One of the major issues is that the synthetic building blocks and very complex aromatic molecular structures of azo-dyes make the substance difficult to overcome. Additionally, their carcinogenic, and tumorigenic impacts coupled with their ability to alter the physicochemical characteristics of the environment require that we treat their effluent to comply with environmental regulations before discharge. For instance, non-reactive, and reactive azodyes have been reported to be toxic to microorganisms such as E. faecalis, V. fischeri, and C. butyricum [12] with orange azodye, and reactive black having EC50 of 15.7 ± 2.68 mg/L, and 11.4 ± 3.68 mg/L respectively. Chung also studied the acute toxicity of original and degraded V5R on marine bioluminescent bacteria Vibrio fischeri, they reported EC50 of 12.73 ± 2.54, and 52.77 ± 3.31 [13] for the undegraded, and degraded V5R respectively, implying that the pristine hydrolyzed V5R was 76% more acute than the photodegraded. In addition to the mentioned toxicity of V5R, it is one of the reactive azodyes which are hard to be biodegraded. The conventional treatment and refined methods for wastewater and other pollutants include biological, coagulation, flocculation, reverse osmosis, nanofiltration, and

* Corresponding author.
E-mail address: stulashie@ucc.edu.gh (S.K. Tulashie).

https://doi.org/10.1016/j.heliyon.2022.e10908
Received 15 January 2022; Received in revised form 25 June 2022; Accepted 28 September 2022

ultrafiltration [14, 15, 16, 17] but are complex and expensive. The drawbacks of biological treatment consisting of low biodegradability, less flexibility in design and operation, larger land area requirements, and longer times required for decolorization-fermentation processes cannot be overlooked [18]. Therefore, other methods such as photodegradation have been explored. For example, Antonio Zuorro et. al, and Chung photocatalytically degraded V5R using Fe-Doped Titania [19], and TiO2 catalysts [13], nonetheless, this method can potentially produce intermediate products which may be more lethal than the pristine V5R [12, 13]. Adsorption with activated carbon is one of the cost-effective, sludge-free, and simple to operate wastewater treatment processes [20, 21, 22]. Thus, the elimination of dyes from wastewater by activated carbon is becoming popular because of its adsorptive efficiency for a wider range of adsorbates [23, 24]. However, commercial activated carbons are comparatively expensive, hence, biochar becomes the alternative for waste treatments [25, 26], especially, in the small local dye industries.

Several researchers have focused on adsorbents to remove dyes and other contaminants from wastewater but at a lower cost of production [27, 28]. Thus biochars from raw materials such as Brazillian pepperwood, coconut coir, Eucalyptus, and palm bark have been applied to remove dyes and other contaminants from aqueous solutions suggesting their potential for reclamation purposes [29, 30, 31]. For instance, the biochars from digestion residues, palm bark, and eucalyptus removed 99.5%, 99.3%, and 86.1% of methylene blue dye with initial concentrations of 5 mg/L [30]. Additionally, biochar from sugarcane bagasse and hickory wood was used to remove sulfamethoxazole with the sugarcane bagasse biochars exhibiting the highest solid-water distribution coefficient of 104L/g [29]. Regarding electroplating wastewater remediation, agro waste, and biochar were applied to remove zinc and lead within possible concentrations of 2.2 g/L and 3.4 g/L whereas poplar sawdust also removed cadmium and lead [32, 33].

Ghana is one of the developing countries whose textile industries hardly treat their dye effluent with effective methods [34]. Akosombo Textile Limited (ATL) is one of the prestigious, largest textile industries in Ghana with a dyeing and finishing capacity of 3 × 106 yards per month [35]. Their effluents, which contain reactive azo dyes, pose threat to the environment, especially, nearby aquatic habitats [34] such as the Volta River and River Densu due to their proximity. Previous studies in Ghana treated the dye effluents with gamma irradiations dose rate of 7.8 kGy/h coupled with chemical treatments using hydrogen peroxide, sodium peroxide, and ferrous ammonium sulphate. Thus, the authors observed improved decoloration of the dye effluent and reduced COD [34]. However, irradiation and chemical treatment could not be affordable in a developing country like Ghana. Therefore, it is necessary to investigate cheaper, but effective, sustainable, and abundant biochar that can be utilized locally to remove the dyes from the textile industry effluent. Converting the readily available local sources such as bamboo and calabash into effective biochar can curb the potential canker when the effluent is exposed to nearby waterbodies. It will also help reduce the cost of the adsorbent. In this paper, we focus on the removal of reactive violet 5 azo dye (V5R) using local bamboo biochar (BB), and calabash biochar (CB). To the best of our knowledge, the kinetics and adsorption of a V5R onto bamboo and calabash biochars have not yet been studied to assess whether BB and CB could be potential adsorbents for reclaiming wastewater contaminated with V5R. V5R was chosen due to its market availability in Ghana and its application in the textile industry. The adsorption equilibria and capacity, as well as the kinetics of BB and CB, will be presented and discussed.

2. Materials and methods

2.1. Sample collection, preparation, and pre-treatment

Dry bamboo and calabash were purchased from the local market at Kotokoraba, Cape Coast-Ghana. We cut the purchased materials into 5 cm × 3 cm average sizes, washed them with distilled water, and sundried them for 24 h. The cut pieces of the dry bamboo and calabash were pyrolyzed in a fixed bed reactor, with a height to diameter ratio of 2:1 (20cm:10cm). They were heated from 20 °C to 500 °C with a heating rate of 10°Cmin-1. The pyrolyzed material was washed with hot distilled water, and oven dried at 120 °C for 48 h. Respective biochar yields of 37% and 48% w/w for bamboo and calabash were attained. The resulting biochars were ground into powder and stored.

2.2. Adsorbate preparation, analytical measurement, and sample characterization

V5R was purchased from another local market in Tema, Accra-Ghana. The V5R has a chemical formula of C20H16N3Na3O15S4 (Figure 1) and CAS number 12226-38-9. It is soluble in water, and has, vibrant violet color. Triplicate melting points were measured using an Electro thermal melting Point Apparatus (Model 1A9100, UK). The melting point was 370.5 ± 5 °C.

The absorbance of V5R was measured via Shimadzu UV-VIS spectrophotometer (Model YUVmini-1240, Japan) to set the baseline wavelength. A peak absorbance of 0.0880 was obtained at 560 nm. Therefore, the characteristic wavelength of $\lambda_{max} = 560$ nm was applied. The calibration curve showed a linear variation of absorbance with R2 of 0.9999. The absorbance was determined using Beer Lambert's Law.

2.3. Specific surface area and pore distribution measurements

Nitrogen adsorption-desorption isotherms were determined for the calabash and bamboo carbon at 76.92 K and 77.01 K, respectively, on the Tristar II adsorption instrument (Tristar II 3020, Micromeritica Instrument Corporation, USA). The N2 adsorption-desorption isotherms were used to determine the Brunauer–Emmett–Teller specific surface area (S_{BET}).

2.4. Fourier transform infrared spectroscopy (FTIR) measurements

The FTIR spectra of the samples were measured between 4000 and 400cm-1 in a Perkin-Elmer Spectrum (Serial number 94133, USA). Sample pressing was done for 4 min in the Perkin-Elmer manual hydraulic press for accurate results.

2.5. Scanning electron microscopy measurements

The biochar morphology was investigated using a scanning electron microscope (SEM) model JSM 6390LV. The surfaces of the biochar powder were coated with a thin layer of platinum using the JS1600 platinum coater, to enhance imaging. Imaging was done in the high vacuum mode under an accelerating voltage of 5 kV. A maximum magnification of 1000 μm was used to capture high-resolution micrographs.

2.6. Batch adsorption procedure and spectrophotometric analysis

Two sets of V5R concentrations of 10–50 mg/L at 10 mg/L intervals were prepared in 50 mL of distilled water. We labeled the resulting solutions as C10, C20, C30, C40, and C50 according to their concentrations. 0.36 g CB was added to each of the resulting solutions, after which the mixture was stirred for 15 min, and the adsorption was allowed to continue until equilibrium. The experiments, as depicted in Figure 2 were performed at the natural pH of V5R, and room temperature of 27 °C. The entire procedure was repeated for BB. The height-to-diameter ratio as indicated in Eq. (1) was 10 (1 m: 0.1 m), and the biochar bed volume reached 1.96×10^{-3} m^3. Additionally, the CB and BB contact time was 10 min and 7 min respectively. Eq. (2) relates the volumetric flowrate contact time and biochar bed volume. The concentrations of V5R at

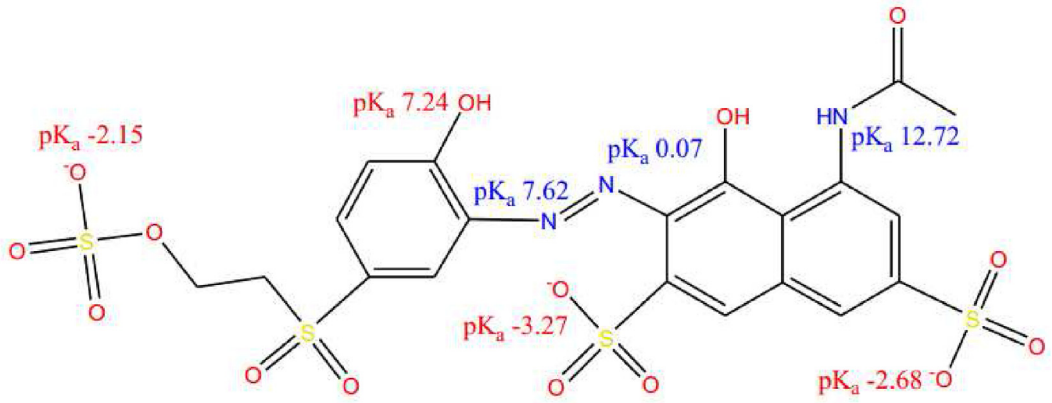

Figure 1. Structures of V5R [36].

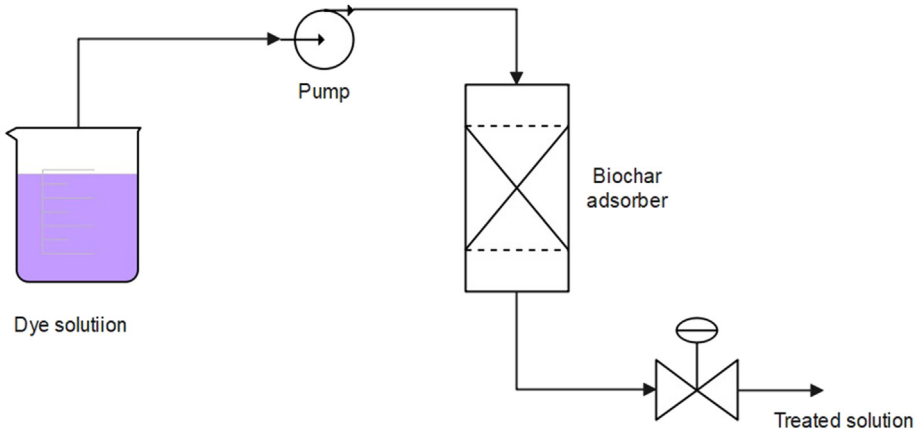

Figure 2. Experimental set-up for treating 10–50 mg/L V5R azo dye solution.

equilibrium were determined by the UV-VIS spectrophotometer at a wavelength of 560 nm. Change the dye effluent the below to solution.

$$\frac{H}{D} = 10 \tag{1}$$

$$Q = \frac{V_b \times 60\ (min/h)}{R_t} \tag{2}$$

Where H, D, Q, Rt, and Vb are biochar bed height (m), biochar bed diameter (m), volumetric flowrate (m3/h), and contact time (min) consecutively.

2.7. Adsorption capacity

The batch adsorption capacity of the biochars was studied, and the equilibrium amount of V5R adsorbed (Xe) was calculated by mass balance (Eqn. 3), considering (V_s).

$$X_e\ (mg/g) = \frac{(C_o - C_e) \times V_s}{m_a} \tag{3}$$

3. Results and discussion

3.1. Characterization of adsorbents

The textural properties of BB and CB are measured by N_2 Adsorption/Desorption isotherms. The dominant pores in BB and CB were mesopores of the corresponding average diameters of 21.1 nm and 26.5 nm. These pore sizes predominantly have an impact on the total adsorption capacities of the BB, and CB. The SBET of the CB and BB is 44.78 m^2/g and 174.67 m^2/g, respectively (Table 1).

3.2. SEM analysis of samples

The surface morphology of the CB and BB were investigated via scanning electron micrographs. The CB (Figure 3 a, b) shows larger granular shapes having pin-holes on the surface whereas the BB micrograph exhibits a closely packed or interconnected structure like a mesh, and is more elongated (Figure 4 a, b).

The structural differences distinguish their adsorptive capacity and specific surface area. Thus, BB has a higher BET specific surface area, hence it is predictably desirable

3.3. FTIR analysis

Employing the FTIR (Figure 5), the surface chemistry of the biochars was determined based on functional groups. The BB shows a very weak broad stretch 3700-3200cm^{-1} corresponding to O–H [37]. The band 2985-2908 cm^{-1}, 1718 cm^{-1}, 1563 cm^{-1} are assigned to the C–H stretch of aldehydes, C=O carboxylic, C=C stretch, respectively [38, 39]. The bands 1074 cm^{-1}, 843.75 cm^{-1}, and 464.53 cm^{-1} are allocated to C–O (in ether, carboxylic, or ester), C–H out of plane bending in the aromatic ring, and C=O bending, respectively [40].

Similar to the BB, surface functional groups present in the CB, the broadband 3000-3500 cm^{-1} corresponds to the O–H group (Figure 6). The O–H band in CB is more visible than in BB, indicating that the bamboo might have a very weak carboxylic group than the calabash. However, CB shows very weak bands at 2980 cm^{-1} and 2900 cm^{-1}, all

Table 1. Kinetic parameters for adsorption of V5R.

C_o (mg/L)	BB					CB				
	10	20	30	40	50	10	20	30	40	50
Xe (exp.) mg/g	1.335	2.711	3.783	4.615	4.923	0.003	0.005	0.0059	0.0060	0.007
1st order pseudo			BB					CB		
Xe (calc.) mg/g	0.500	0.797	2.379	2.808	3.107	0.003	0.009	0.0079	0.0230	0.0297
k_1 (h^{-1})	0.694	0.495	0.480	0.467	0.455	1.232	1.106	0.592	0.566	0.526
R^2	0.991	0.951	0.986	0.941	0.930	0.931	0.891	0.955	0.926	0.957
2nd order pseudo										
Xe (calc.) mg/g	1.402	2.761	4.179	4.916	5.219	0.004	0.007	0.009	0.010	0.013
k_2 (g/mgh)	2.336	1.339	0.407	0.286	0.241	85.43	37.14	29.35	32.69	22.28
h (mg/gh)	4.596	10.204	7.112	6.901	6.562	0.002	0.002	0.003	0.004	0.004
R^2	0.999	0.999	0.998	0.987	0.981	0.972	0.988	0.987	0.987	0.964
Intraparticle diffusion										
k_d ($mg/gh^{1/2}$)	0.270	0.744	1.098	1.239	1.420	0.001	0.003	0.003	0.004	0.005
z_i	0.816	1.410	1.603	1.787	1.643	0.00004	0.0013	0.0007	0.0009	0.0016
R^2	0.997	0.999	0.994	0.981	0.967	0.9969	0.9878	0.9968	0.9997	0.9930

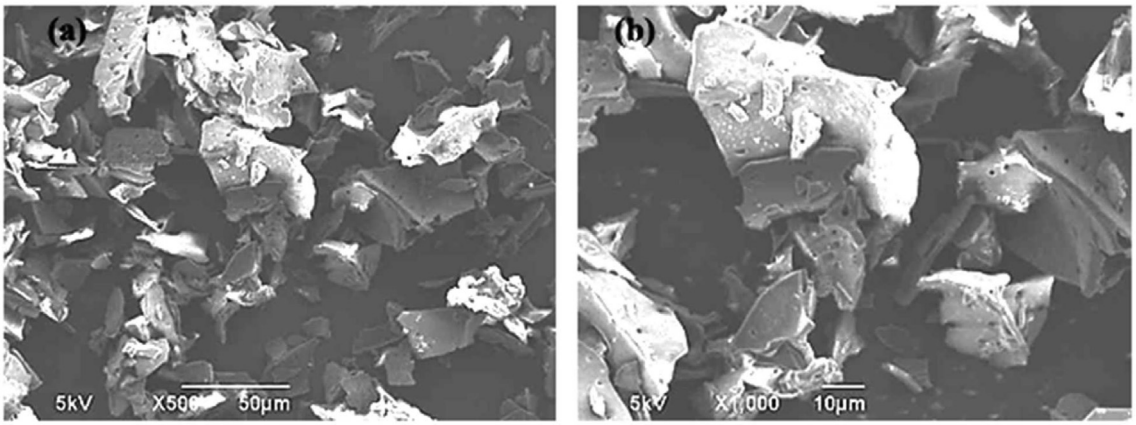

Figure 3. SEM micrograph of calabash activated carbon **(a)** x500, **(b)** x1000 magnification.

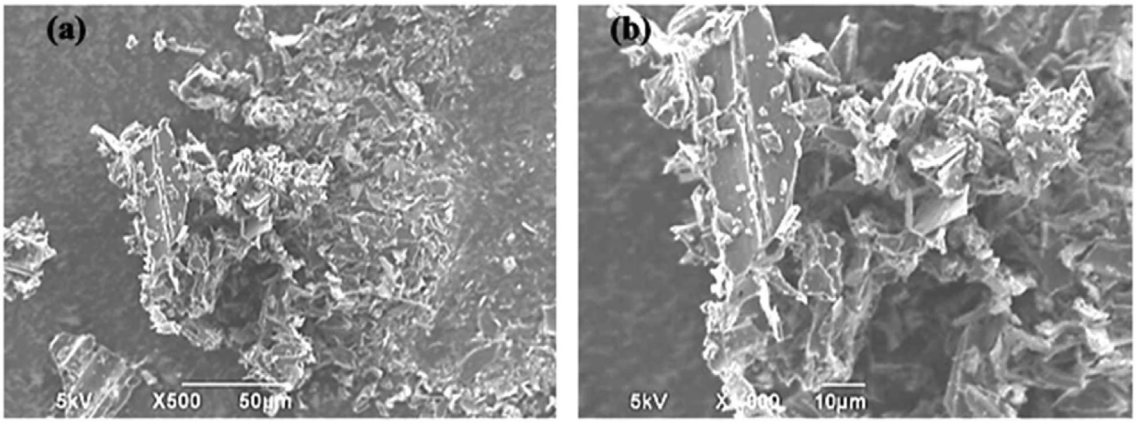

Figure 4. SEM micrograph of bamboo biochar (**a**) x500, (**b**) x1000 magnification.

corresponding to the C–H stretch. The 1577.05 cm^{-1}, 1215.97 cm^{-1}, and 811.57 are assigned to C=C, C–O, and C–H out of plane bending in the aromatic ring.

The FTIR spectrum of the V5R (Figure 7) shows 3200-3600 cm^{-1} broad stretch, 1615.85 cm^{-1}, stretch 1548 cm^{-1}, 1303 cm^{-1} and 1183 cm^{-1} which correspond to O–H, aromatic C=C stretch, N=N, and S–O(SO_3–H) stretch sequentially [41, 42, 43].

3.4. Effect of contact time on adsorption of V5R onto BB and CB

We studied the adsorption rate from 0 to 7 h. In all concentrations, a rapid adsorption rate by the BB occurs within 1 h after which the BB gradually adsorbs the V5R (Figure 8). At 1 h, the BB adsorbs the V5R maximum by 78% and 46.2% in C10, and C50, respectively. The fast adsorption of the V5R by the biochar at the initial stage can be attributed

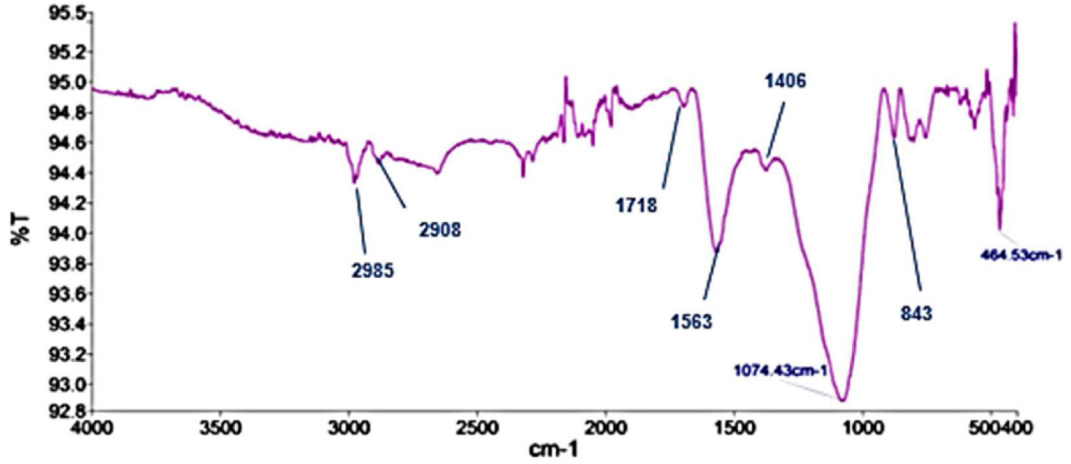

Figure 5. FTIR spectrum of BB.

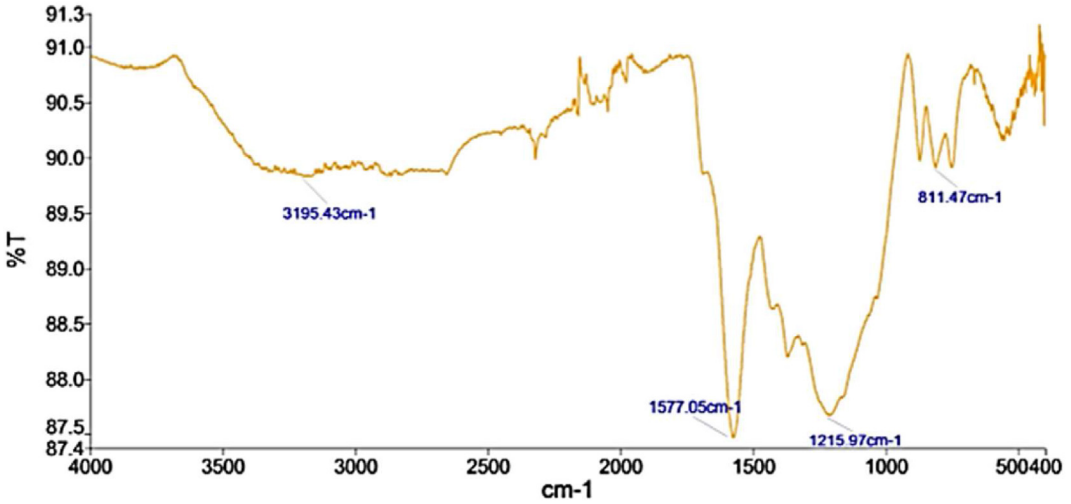

Figure 6. FTIR spectrum of CB.

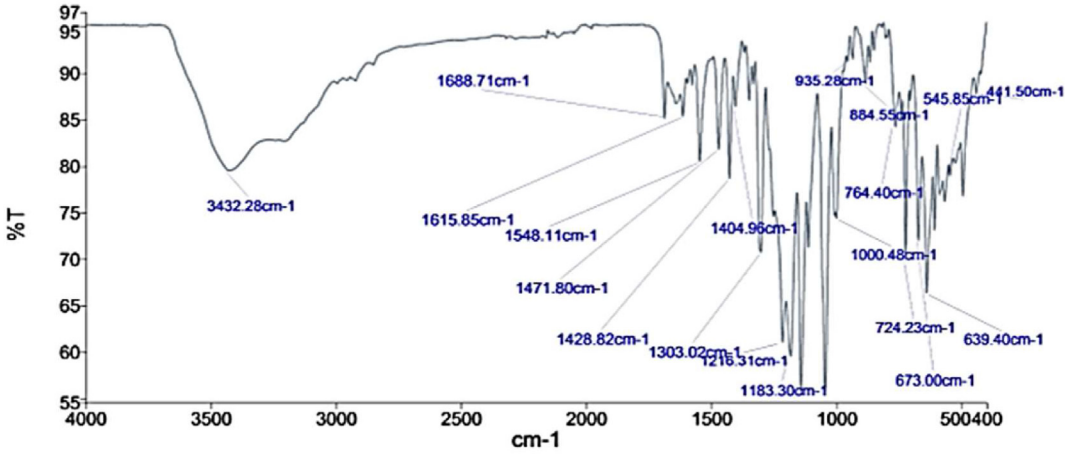

Figure 7. FTIR spectrum of V5R dye.

to the abundance of free active sites interacting with the V5R. The adsorption of C10, and C20 reaches equilibrium at 3–4 h whereas C30, C40, and C50 attain at 5 h. The BB gradually adsorbs the C40 and C50 at 2–4 h before reaching equilibrium.

The CB adsorbs the C10 rapidly at 1 h and slows down to equilibrium at 6 h. Rapid adsorption of C20 and C30 continues until the 6 h where equilibrium is established (Figure 9). The C40 and C50 are quickly adsorbed within the first 4 h, then retards to equilibrium at 6 h. Like the

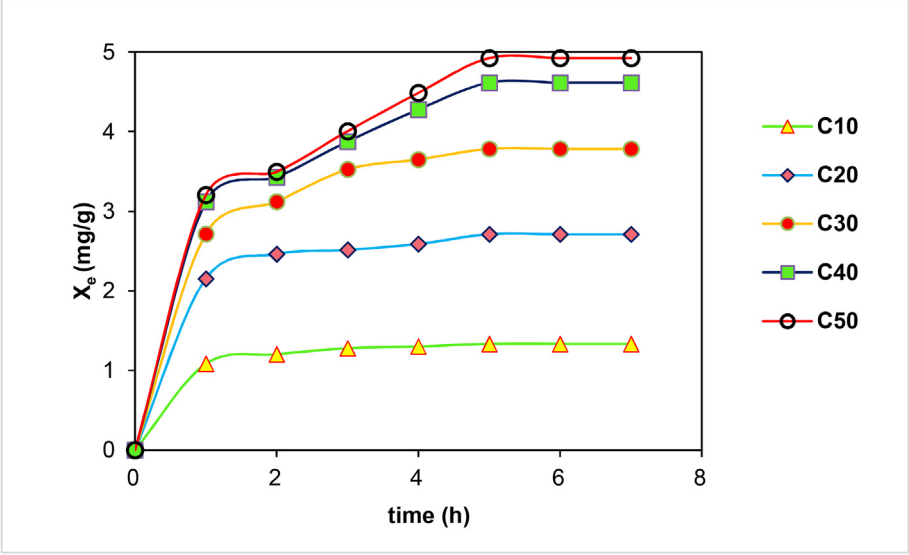

Figure 8. Effect of contact time on adsorption of V5R onto 0.36g of BB activated carbon.

BB, all adsorption of V5R by CB retards gradually before reaching equilibrium.

Nevertheless, the CB adsorbs only 0.1–0.2% of V5R throughout the studied period. However, as the adsorption proceeds, the V5R rapidly occupies the available active sites, eventually slowing down the process. The BB and CB absorptive equilibrium at 27 °C is lower than the adsorption of V5R by cocoa pod biochar reported being 12.99 mg/g at 30 °C [44]. Other authors also removed Basic Red 46, and Reactive Black 5 (RB5) dye from aqueous solutions using bamboo, and banana peel biochars, reporting adsorption capacities of 9.06 mg/g and 7.58 mg/g respectively [45, 46]. However, it is important to note that the variations in the various adsorption capacities compared to this study could be attributed to different temperatures and pH of the solutions used in the other studies. For instance, the V5R adsorption on the cocoa pod increased fourfold (52.63 mg/g) when the temperature was 45 °C and was reported to be more favorable in acidic conditions [44].

3.5. Effects of initial adsorbate concentration on quantity adsorbed at equilibrium

Generally, when initial concentration increases, both biochars absorb more V5R (Figure 10). However, percentage adsorption at equilibrium decreases as a larger quantity of Co is added. At equilibrium, the BB ultimately adsorbs 96% and 70.9% of 10 mg/L and 50 mg/L V5R Co, sequentially but the CB adsorbs only 0.1–0.2% which may be attributed to the poor affinity between CB and V5R compared to BB. The reduction in percentage adsorption can be attributed to the inadequate active sites for the V5R adsorption.

3.6. Adsorption kinetics

We applied the pseudo-first-order (Eqn. 4), pseudo-second-order (Eqn. 5), and intraparticle diffusion (Eqn. 6) models to predict the sorption kinetics [47]. The adsorption rate constants k_1 and k_2 are sequentially calculated from the slope of the plot $\ln(X_e - X_t)$ versus time t, and the intercept of the plot of $\frac{t}{X_t}$ against t. The intraparticle diffusion rate constant (k_d) and its corresponding boundary layer thickness parameter (z_i) relate to the quantity of sorbate adsorbed at a given time (X_t) as expressed in (Eqn. 6). The initial adsorption rate, h, is expressed as a function of the pseudo-second-order rate constant (Eqn. 7).

$$\ln(X_e - X_t) = k_1 t + \ln X_e \tag{4}$$

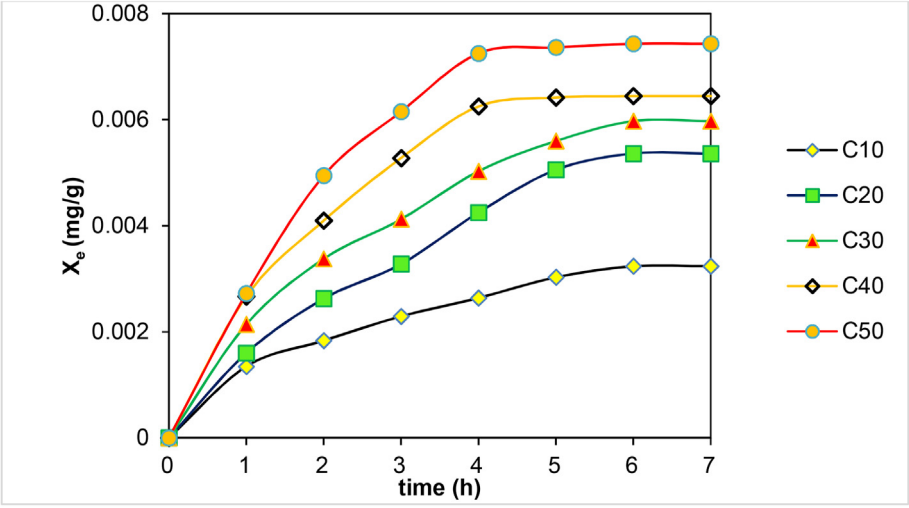

Figure 9. Impact of contact time on adsorption of V5R onto 0.36g of CB activated carbon.

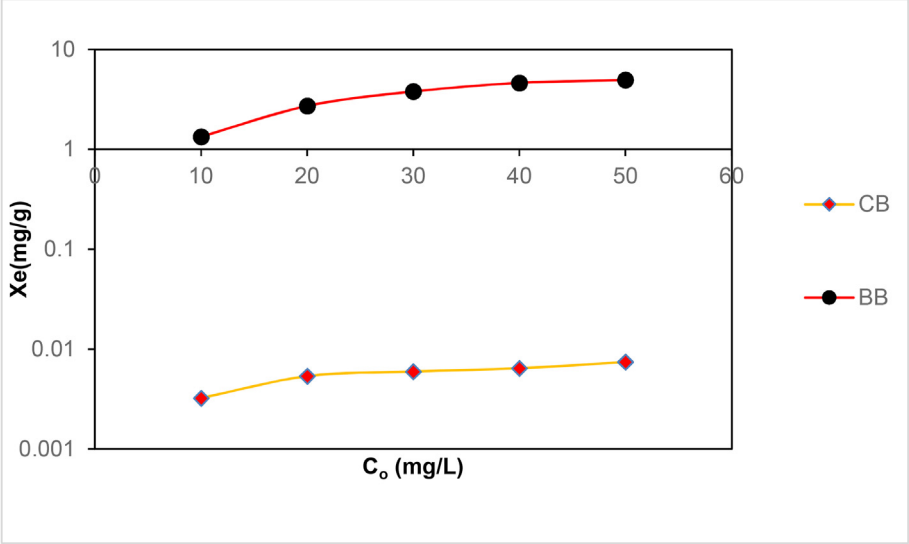

Figure 10. Impact of initial concentration on V5R adsorbed at equilibrium.

$$\frac{t}{X_t} = \frac{1}{X_e}t + \frac{1}{k_2 X_e^{\,2}} \tag{5}$$

$$X_t = k_d t^{1/2} + z_i \tag{6}$$

$$h = k_2 X_e^{\,2} \tag{7}$$

Generally, increasing the initial concentration of V5R reduces both the pseudo-first-order and pseudo-second-order constants (Table 1). The sorption kinetics fit best for the pseudo-second-order kinetic model with R^2 range of 0.981–0.999, and 0.913–0.987 for BB and CB, respectively.

The intraparticle diffusion rate constant and its corresponding boundary layer thickness parameter (z_i) increase as C_o rises. z_i becomes zero if the limiting step is only intraparticle diffusion [47]. Thus, if film diffusion plays a major role, Eq. (6) does not cross the origin, $z_i \neq 0$ (Figure 11). In this study, the intraparticle diffusion and film diffusion influence the adsorption rate in both BB and CB, however lower values of z_i in CB indicate that CB has less film diffusion resistance than BB. The results agree with other studies conducted on Juglans regia, and fly ash [48]. Figures 11 and 12 confirm the trend and the rate at which the BB, and CB absorb the V5R as already described in Figures 8, and 9, sequentially.

3.7. The adsorption isotherms

Our study covers the non-linear fitting of Langmuir, Freundlich, Redlich Peterson, and Sips isotherms with the experimental results using an excel solver. These isotherms have been used to describe the equilibrium characteristics of the V5R adsorption onto BB, and CB.

The Langmuir isotherm is a two-parameter model which expresses the equilibrium characteristics during monolayer adsorption. It relates the equilibrium concentration to the maximum quantity adsorbed (Xmax), the quantity adsorbed at equilibrium, XeLM (Eqn. 8). The Langmuir equilibrium parameter, RLM (Eqn. 9), indicates whether the adsorption is irreversible (RLM = 0), favorable (0<RLM<1), linear (RLM = 1) or unfavorable (RLM>1) [49].

$$X_{eLM} = \frac{X_{max}\, K_{LM} C_e}{1 + K_{LM} C_e} \tag{8}$$

Where K_{LM} is Langmuir constant (L/g)

$$R_{LM} = \frac{1}{1 + K_{LM} C_o} \tag{9}$$

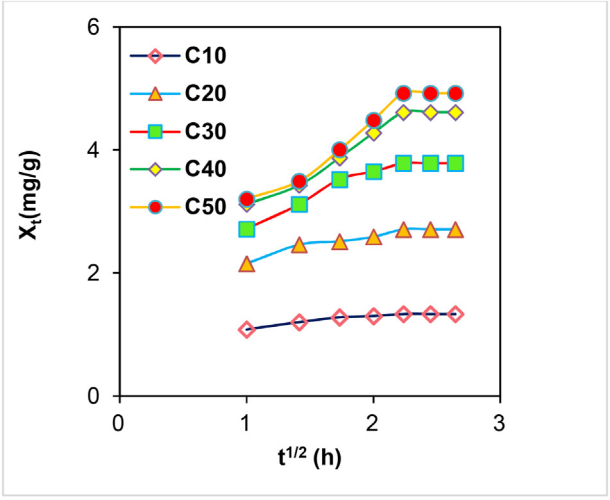

Figure 11. Intraparticle diffusion model for BB.

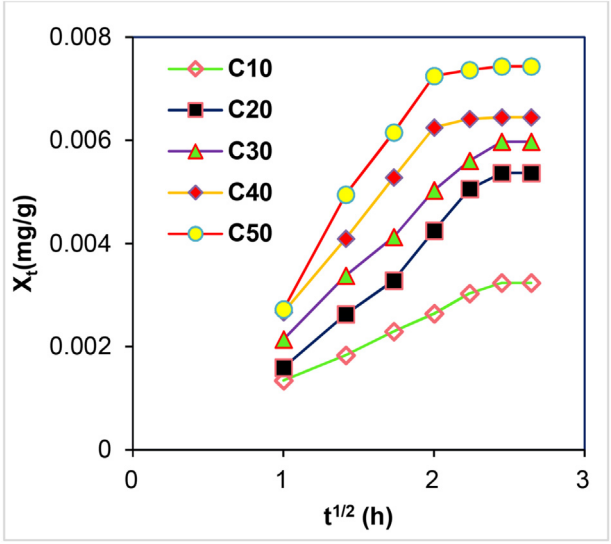

Figure 12. Intraparticle diffusion model for CB.

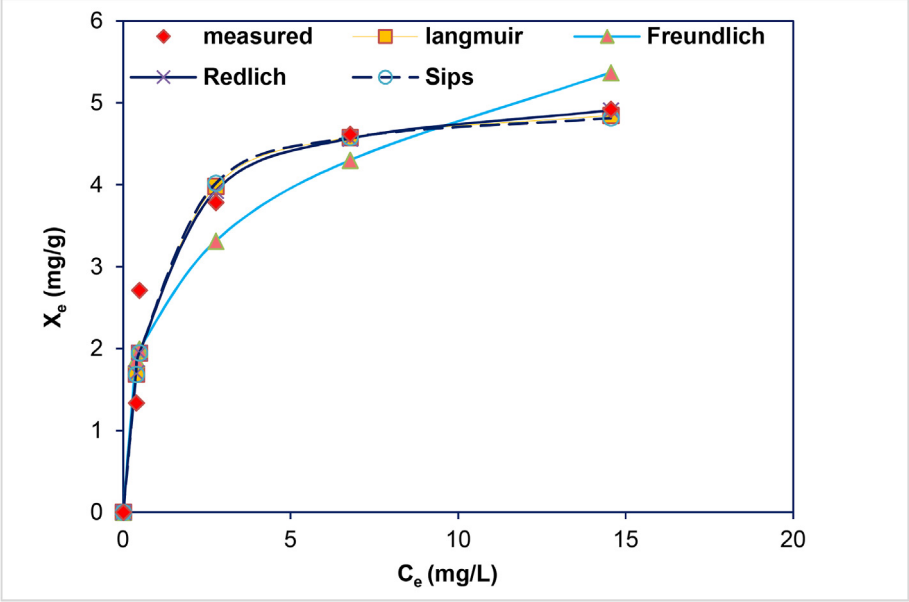

Figure 13. Nonlinear fitting of models to experimental data from BB.

Freundlich isotherm is an empirical equilibrium description of adsorption on a heterogeneous surface, and it expresses the quantity sorbed at equilibrium (X_{eFD}) as a function of equilibrium concentration (Eqn. 10). The Freundlich parameters, b, and K_{FD} reflect the extent of adsorption affinity or nonlinearity between C_e and X_{eFD} [50].

$$X_{eFD} = K_{FD} C_e^{1/b} \tag{10}$$

Redlich-Peterson model incorporates both Langmuir and Freundlich isotherms, making it versatile for both homogeneous and heterogeneous surfaces. The equilibrium quantity adsorbed (X_{eRP}) relates to the Redlich-Peterson constant, K_{RP}, and parameters α, and β as shown in Egn.11. It reduces to Langmuir when $\beta = 1$ (at low concentrations) and minimizes to Freundlich when $\beta = 0$ (at high concentrations).

$$X_{eRP} = \frac{\alpha C_e}{1 + K_{RP} C_e^{\beta}} \tag{11}$$

Sips isotherm, like Redlich-Peterson comprises both Langmuir and Freundlich isotherms. Sips equilibrium quantity adsorbed (X_{eSips}) simplifies to Langmuir when $\gamma = 1$ but reduces to Freundlich isotherm when C_e is very high. Eq. (12) links X_{eSips} to the Sips parameters A, γ, and constant K_{SP}.

$$X_{eSips} = \frac{A C_e^{\gamma}}{1 + K_{SP} C_e^{\gamma}} \tag{12}$$

The χ^2 error function indicates that the Redlich-Peterson, Sips, and Langmuir models all fit well with the experimental data (Figure 13) obtained from the V5R sorption on bamboo.

Table 2. Fitting parameters and equilibrium amount of V5R adsorbed.

C_o(mg/L)	BB					CB				
	10	20	30	40	50	10	20	30	40	50
Xe (exp.) mg/g	1.335	2.711	3.783	4.615	4.923	0.003	0.005	0.006	0.006	0.007
Langmuir					Parameters					Parameters
X_{max} (mg/g)					5.106					0.010
K_{LM} (L/g)					1.285					0.049
R_{LM}					0.940					0.998
χ^2					0.323					4.36E-05
Freundlich					Parameters					Parameters
K_{FD} (L/g)$^{1/b}$					2.466					0.001
b					3.441					2.113
χ^2					0.525					8.39E-05
Redlich-Peterson					Parameters					Parameters
β					0.973					1.078
α (L/g)					6.934					0.0005
K_{RP} (L/mg)$^{\beta}$					1.443					0.033
χ^2					0.321					4.28E-05
Sips					Parameters					Parameters
K_{SP} (L/mg)$^{\gamma}$					1.372					0.036
γ					1.050					1.021
A (L/g)$^{\gamma}$					6.896					0.0003
χ^2					0.322					4.01E-05

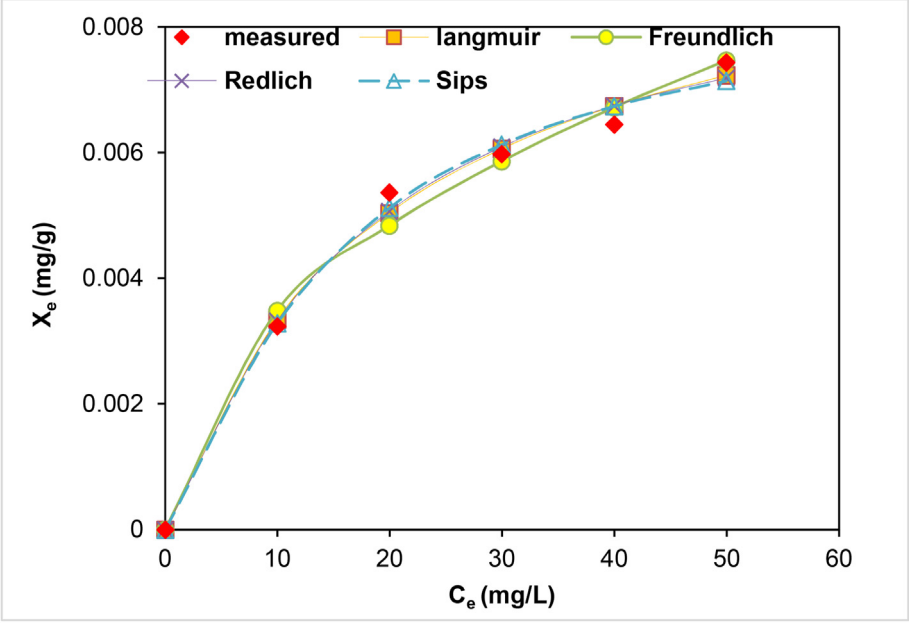

Figure 14. Nonlinear fitting of models to experimental data from CB.

However, the respective β and γ values (Table 2) in Redlich-Peterson and Sips are both closer to 1, hence, they reduce to the Langmuir model, representing monolayer adsorption. Besides, RLM = 0.940 depicts that Langmuir isotherm is more favorable. The Sips', and Redlich-Peterson's maximum adsorption capacity ($A/K_{SP,}$ and $\alpha^{\beta}/K_{RP,}$ respectively) re 98.4% and 94.1% consistent with Langmuir's (Xmax = 5.106 mg/g) sequentially.

Like the BB, Redlich-Peterson, Sips, and Langmuir models fit well with the experimental data obtained from calabash adsorbent (Figure 14). Nonetheless, the Sips model shows the strongest agreement with the data but also reduces to Langmuir ($X_{max} = 0.010$) since $\gamma \sim 1$. In all adsorption cases, Freundlich isotherm demonstrated the least fit. This implies that the adsorption of V5R by bamboo and calabash is a monolayer and occurs on a homogeneous surface.

3.8. Possible adsorption mechanisms

The FTIR peaks (Figure 7) at 1718 cm^{-1}(C=O), and 1074 cm^{-1} (C–O bending) are associated with the oxygenated sites of the carbonyl, esters, or carboxylic groups on the BB. The V5R structure (Figure 1, and Figure 7) and has aromatic rings with hydroxyl, oxyl, amine, and sulphonic groups attached. Therefore, there are possible interactions between the V5R aromatic rings, hydroxyl, oxyl, amine, or sulphonic groups, and the oxygenated sites of the carbonyl, esters, or carboxylic acids [51] on the BB heterogeneous surface via a donor-acceptor mechanism. Additionally, the formation of water cluster, in other words, the water adsorption mechanism via hydrogen bonding to the oxygenated sites [51, 52] of the BB may largely influence the V5R adsorption. Nevertheless, it is important to note that the donor-acceptor and water adsorption mechanisms exhibiting the impact of the oxygenated sites can be confirmed with certainty if the adsorption is further studied separately in media other than water, such as air, N_2, and cyclohexane [52]. After the oxygenated sites are exhausted, possible dispersive interactions of the V5R with the BB carbon basal planes are feasible. However, with the BB exhibiting substantial BET surface area (174.67 m^2/g) within the range (16.90–350 m^2/g) reported in literature [53, 54, 55], its low adsorptive capacity (5.106 mg/g) observed from the sorption isotherm indicates

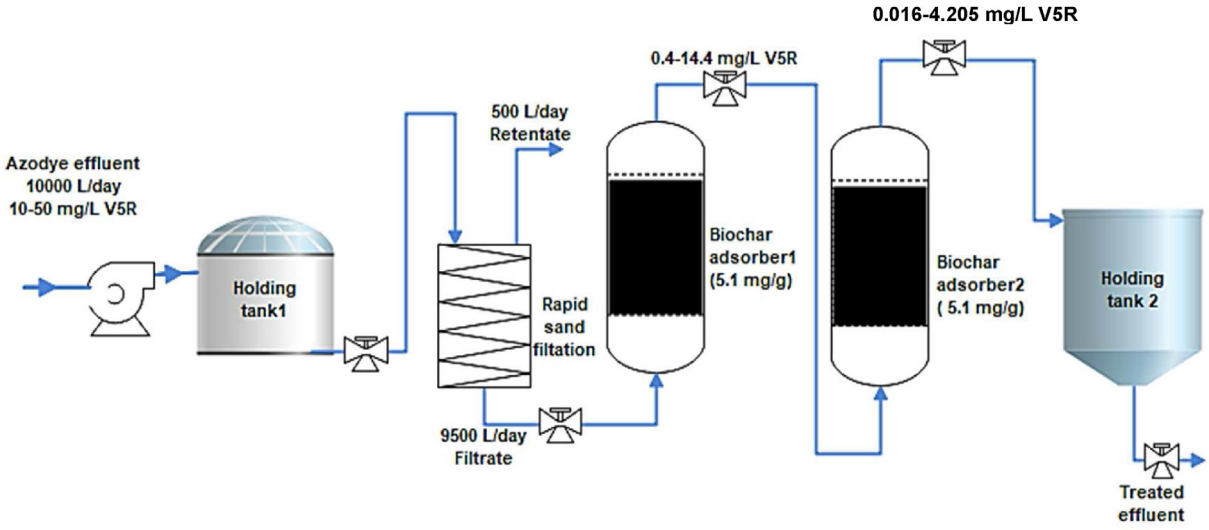

Figure 15. Prototype for eliminating 99.8% of 10 mg/L, and 91.6% of 50 mg/L V5R azo dye.

that water adsorption mechanism potentially impacted greatly the V5R adsorption to BB.

3.9. Proposal of a treatment model

From the results of this study, a novel remedy prototype (Figure 15) is presented to treat the textile effluent containing the azo dye contaminant. This prototype of Figure 2 (experimental model set up) includes the bamboo biochar (BB) incorporated in the adsorption columns, holding tanks, rapid sand filters, valves, and pumps. The BB is selected because it demonstrates a better adsorptive capacity compared with CB.

The 15000 L capacity Holding tank 1 receives the 10000 L effluent which contains 10–50 mg/L V5R. The rapid sand filter eliminates suspended particles which can interfere with the adsorptive capacity of the biochar. Each of the BB in absorbers 1 and 2 with an adsorptive capacity of 5.1 mg/g removes 96% of the 10 mg/L, and 71 % of the 50 mg/L V5R azo dye emanating from the sand filter. Thus, absorber 1 has a capacity range of 18.63 kg–93.14 kg BB considering the 10–50 mg/L V5R azo dye. The absorber 2 treats the remaining 4%–29% of the V5R azo dye, requiring 0.745 kg–27.0 kg BB, leaving only 0.016 mg/L-4.205 mg/L V5R in the exit stream to the Holding tank 2 where we will further monitor the key parameters to determine their suitability for discharge, otherwise, it will be recycled for retreatment. Eventually, the two adsorption columns potentially eliminate 99.8 % of the 10 mg/L and 91.6 % of the 50 mg/L, making it feasible for treating 10–50 mg/L V5R. This remediation approach is very sustainable due to the proliferation and abundance of bamboo, making the BB readily available for use.

4. Conclusion

Bamboo and calabash biochar (BB, and CB) are employed to treat 10–50 mg/L Reactive Violet 5 (V5R) contaminant. The adsorption rates are consistent with pseudo-second-order kinetics. The rate constant, k2, for BB, and CB decreases by 89.7% and 83.3%, respectively, starting from 2.34 g/mgh and 85.43 g/mgh. Increasing the initial concentration of V5R increases the boundary layer thickness parameter (zi), and the intra-particle diffusion rate constant. The intraparticle diffusion dominates the adsorption rate in BB than the CB but film diffusion limits the mass transfer in BB than CB since the diffusion boundary layer thickness constant (zi) in CB is lower than in BB. Rapid adsorption generally dominates both BB and CB within 1 h due to the availability of more active sites, reaching equilibrium at 3–6 h. The adsorption of V5R by BB, and CB follows Langmuir, Redlich-Peterson, and Sips isotherms better than Freundlich. Nevertheless, the respective Redlich-Peterson β, and Sips γ parameters are all closer to 1, hence they reduce to Langmuir's model. Similarly, the Langmuir parameter, RLM, in both BB and CB is less than 1, which affirms that the Langmuir isotherm is favorable. Therefore, at 10–50 mg/L V5R, the BB respectively adsorbs 71%–96% of V5R at equilibrium whereas CB adsorbs only 0.1–0.2% due to the lower affinity between CB and V5R. The results suggest that bamboo biochar can potentially reduce 10–50 mg/L of V5R in textile effluent to a range of 4–29%, thereby, making bamboo a potential adsorbent for eliminating V5R in textile effluent. The prototype is expected to remove 99.8% of 10 mg/L, and 91.6% of the 50 mg/L V5R, hence, may be suitable for V5R azo dye textile effluent remediation.

Declarations

Author contribution statement

Samuel Tulashie; Francis Kotoka: Conceived and designed the experiments; Analyzed and interpreted the data; Contributed reagents, materials, analysis tools or data; Wrote the paper.

Bennett Nana Botchway: Performed the experiments; Analyzed and interpreted the data; Contributed reagents, materials, analysis tools or data; Wrote the paper.

Kofi Adu: Analyzed and interpreted the data; Contributed reagents, materials, analysis tools or data.

Funding statement

This research did not receive any specific grant from funding agencies in the public, commercial, or not-for-profit sectors.

Data availability statement

Data included in article/supp. material/referenced in article.

Declaration of interest's statement

The authors declare no conflict of interest.

Additional information

No additional information is available for this paper.

Acknowledgements

The authors are grateful to the University of Cape Coast, Ghana for their support. We are also grateful to Dr. Juliet Ewool at University of Ghana, Legon for the support in the SEM measurements.

References

[1] N. Gómez, M.V. Sierra, A. Cortelezzi, A. Rodrigues Capítulo, Effects of discharges from the textile industry on the biotic integrity of benthic assemblages, Ecotoxicol. Environ. Saf. 69 (2008) 472–479.
[2] J.O. V, M. BN, Toxicity assessment of treated effluents from a textile industry in Lagos, Nigeria, Afr. J. Environ. Sci. Technol. 6 (2012) 438–445.
[3] S. S, B. LG, Removal of Dyes from Wastewater Using Adsorption - A Review, 2009.
[4] M. Sudha, A. Saranya, G. Selvakumar, N. Sivakumar, Microbial degradation of azo dyes: a review, Int. J. Curr. Microbiol. App. Sci. 3 (2014) 670–690.
[5] A. Baban, A. Yediler, D. Lienert, et al., Ozonation of high strength segregated effluents from a woollen textile dyeing and finishing plant, Dyes Pigments 58 (2003) 93–98.
[6] S.K. Sen, S. Raut, P. Bandyopadhyay, S. Raut, Fungal decolouration and degradation of azo dyes: a review, Fungal Biol. Rev. 30 (2016) 112–133.
[7] M. Solís, A. Solís, H.I. Pérez, et al., Microbial decolouration of azo dyes: a review, Process Biochem. 47 (2012) 1723–1748.
[8] M. Javaid Mughal, R. Saeed, M. Naeem, et al., Dye fixation and decolourization of vinyl sulphone reactive dyes by using dicyanidiamide fixer in the presence of ferric chloride, J. Saudi Chem. Soc. 17 (2013) 23–28.
[9] H.S. Rai, M.S. Bhattacharyya, J. Singh, et al., Removal of Dyes from the Effluent of Textile and Dyestuff Manufacturing Industry: A Review of Emerging Techniques with Reference to Biological Treatment, 2007.
[10] M.C. Somasekhara Reddy, L. Sivaramakrishna, A. Varada Reddy, The use of an agricultural waste material, Jujuba seeds for the removal of anionic dye (Congo red) from aqueous medium, J. Hazard Mater. 203 (204) (2012) 118–127.
[11] C.A.P. Almeida, N.A. Debacher, A.J. Downs, et al., Removal of methylene blue from colored effluents by adsorption on montmorillonite clay, J. Colloid Interface Sci. 332 (2009) 46–53.
[12] A. Gottlieb, C. Shaw, A. Smith, et al., The toxicity of textile reactive azo dyes after hydrolysis and decolourisation, J. Biotechnol. 101 (2003) 49–56.
[13] Y.C. Chung, C.Y. Chen, Degradation of azo dye reactive violet 5 by TiO2 photocatalysis, Environ. Chem. Lett. 7 (2009) 347–352.
[14] S. Beier, S. Köster, K. Veltmann, et al., Treatment of hospital wastewater effluent by nanofiltration and reverse osmosis, Water Sci. Technol. 61 (2010) 1691–1698.
[15] S. Suarez, J.M. Lema, F. Omil, Pre-treatment of hospital wastewater by coagulation–flocculation and flotation, Bioresour. Technol. 100 (2009) 2138–2146.
[16] S. Babel, T.A. Kurniawan, Low-cost adsorbents for heavy metals uptake from contaminated water: a review, J. Hazard Mater. 97 (2003) 219–243.
[17] F. Kotoka, S.K. Tulashie, D.D. Setsoafia, Production of Bioethanol from Liquid Waste from Cassava Dough during Gari Processing, 2017.
[18] R. Fba, Removal of dyes form textile wastewater by adsorption using shrimp shell, Int. J. Waste Res. 6 (2016) 3.
[19] A. Zuorro, R. Lavecchia, M.M. Monaco, et al., Photocatalytic degradation of azo dye reactive violet 5 on Fe-doped Titania catalysts under visible light irradiation, Catalyst 9 (2019) 645, 645 9.
[20] S.K. Tulashie, F. Kotoka, F.K. Kholi, et al., Assessment and remediation of pollutants in Ghana's Kete-Krachi District Hospital effluents using granular and smooth activated carbon, Heliyon 4 (2018) 692.
[21] I.N. Najm, V.L. Snoeyink, B.W. Lykins, J.Q. Adams, Using powdered activated carbon: a critical review, J. Am. Water Works Assoc. 83 (1991) 65–76.

[22] A. Bielski, Models of adsorption of natural contaminants from treated water for municipal purposes on powdered activated carbon, Tech. Trans. (2020) 1–14.
[23] N.A. Dahlan, L.W. Lee, J. Pushpamalar, S.L. Ng, Adsorption of methylene blue onto carboxymethyl sago pulp-immobilized sago waste hydrogel beads, Int. J. Environ. Sci. Technol. 16 (2019) 2047–2058.
[24] S. Natarajan, H.C. Bajaj, R.J. Tayade, Recent advances based on the synergetic effect of adsorption for removal of dyes from waste water using photocatalytic process, J. Environ. Sci. 65 (2018) 201–222.
[25] W. Xiang, X. Zhang, J. Chen, et al., Biochar technology in wastewater treatment: a critical review, Chemosphere 252 (2020), 126539.
[26] N. Hagemann, K. Spokas, H.P. Schmidt, et al., Activated carbon, biochar and charcoal: linkages and synergies across pyrogenic carbon's ABCs, Water 10 (2018) 182, 182 10.
[27] U.J. Etim, S.A. Umoren, U.M. Eduok, Coconut coir dust as a low cost adsorbent for the removal of cationic dye from aqueous solution, J. Saudi Chem. Soc. 20 (2016) S67–S76.
[28] S.M. Kanawade, R.W. Gaikwad, Removal of methylene blue from effluent by using activated carbon and water hyacinth as adsorbent, Int. J. Chem. Eng. Appl. (2011) 317–319.
[29] Y. Yao, B. Gao, H. Chen, et al., Adsorption of sulfamethoxazole on biochar and its impact on reclaimed water irrigation, J. Hazard Mater. 209 (2012) 408–413, 210.
[30] L. Sun, S. Wan, W. Luo, Biochars prepared from anaerobic digestion residue, palm bark, and eucalyptus for adsorption of cationic methylene blue dye: characterization, equilibrium, and kinetic studies, Bioresour. Technol. 140 (2013) 406–413.
[31] Y.S. Shen, S.L. Wang, Y.M. Tzou, et al., Removal of hexavalent Cr by coconut coir and derived chars – the effect of surface functionality, Bioresour. Technol. 104 (2012) 165–172.
[32] R. Gayathri, K.P. Gopinath, P.S. Kumar, Adsorptive separation of toxic metals from aquatic environment using agro waste biochar: application in electroplating industrial wastewater, Chemosphere 262 (2021), 128031.
[33] S. Cheng, Y. Liu, B. Xing, et al., Lead and cadmium clean removal from wastewater by sustainable biochar derived from poplar saw dust, J. Clean. Prod. 314 (2021), 128074.
[34] Dogbe SA, Emi-Reynolds G, Banini GK. EFFECTS OF RADIATION ON WASTEWATER FROM 5 TEXTILE INDUSTRIES IN GHANA. https://inis.iaea.org/collection/NCLCollectionStore/_Public/32/037/32037233.pdf. (Accessed 9 August 2022).
[35] Akosombo Textile Limited, Dyeing and Finishing Capacity, 2022. http://www.cmtgo.com/factory/factory_atl.htm. (Accessed 9 August 2022).
[36] L. Sellaoui, É.C. Lima, G.L. Dotto, et al., Physicochemical modeling of reactive violet 5 dye adsorption on home-made cocoa shell and commercial activated carbons using the statistical physics theory, Results Phys. 7 (2017) 233–237.
[37] Z. Ma, D. Chen, J. Gu, et al., Determination of pyrolysis characteristics and kinetics of palm kernel shell using TGA–FTIR and model-free integral methods, Energy Convers. Manag. 89 (2015) 251–259.
[38] Z. Ma, Q. Sun, J. Ye, et al., Study on the thermal degradation behaviors and kinetics of alkali lignin for production of phenolic-rich bio-oil using TGA–FTIR and Py–GC/MS, J. Anal. Appl. Pyrolysis 117 (2016) 116–124.
[39] D. Chen, D. Liu, H. Zhang, et al., Bamboo pyrolysis using TG–FTIR and a lab-scale reactor: analysis of pyrolysis behavior, product properties, and carbon and energy yields, Fuel 148 (2015) 79–86.
[40] K.A. Vijayalakshmi, K. Vignesh, N. Karthikeyan, Synthesis and Surface Characterisation of Bamboo Charcoal Carbon Using Low Temperature Plasma Treatment, 2015.
[41] F. Ahmed, R. Dewani, M.K. Pervez, et al., Non-destructive FT-IR analysis of mono azo dyes, Bulg. Chem. Commun. 48 (2016) 71–77.
[42] M.C. Grieve, R.M.E. Griffin, R. Malone, Characteristic dye absorption peaks found in the FTIR spectra of coloured acrylic fibres, Sci. Justice 38 (1998) 27–37.
[43] M.M. Aftan, M.A. Toma, A.H. Dalaf, et al., Synthesis and characterization of new azo dyes based on thiazole and assess the biological and laser efficacy for them and study their dyeing application, Egypt. J. Chem. 64 (2021) 2903–2911.
[44] O.S. Bello, T.T. Siang, M.A. Ahmad, Adsorption of Remazol Brilliant Violet-5R reactive dye from aqueous solution by cocoa pod husk-based activated carbon: kinetic, equilibrium and thermodynamic studies, Asia Pac. J. Chem. Eng. 7 (2012) 378–388.
[45] E.A. Sackey, Y. Song, Y. Yu, H. Zhuang, Biochars derived from bamboo and rice straw for sorption of basic red dyes, PLoS One 16 (2021), e0254637.
[46] R.T. Kapoor, M. Rafatullah, M.R. Siddiqui, et al., Removal of reactive black 5 dye by banana peel biochar and evaluation of its phytotoxicity on tomato, Sustain. Times 14 (2022) 4176, 4176 14.
[47] T. Bohli, A. Ouederni, N. Fiol, I. Villaescusa, Evaluation of an activated carbon from olive stones used as an adsorbent for heavy metal removal from aqueous phases, Compt. Rendus Chem. 18 (2015) 88–99.
[48] V. Vadivelan, K. Vasanth Kumar, Equilibrium, kinetics, mechanism, and process design for the sorption of methylene blue onto rice husk, J. Colloid Interface Sci. 286 (2005) 90–100.
[49] S. Nethaji, A. Sivasamy, A.B. Mandal, Adsorption isotherms, kinetics and mechanism for the adsorption of cationic and anionic dyes onto carbonaceous particles prepared from Juglans regia shell biomass, Int. J. Environ. Sci. Technol. 10 (2013) 231–242.
[50] M. Belhachemi, F. Addoun, Comparative adsorption isotherms and modeling of methylene blue onto activated carbons, Appl. Water Sci. 13 (1) (2011) 111–117.
[51] R.W. Coughlin, F.S. Ezra, Role of surface acidity in the adsorption of organic pollutants on the surface of carbon, Environ. Sci. Technol. 2 (1968) 291–297.
[52] M. Franz, H.A. Arafat, N.G. Pinto, Effect of chemical surface heterogeneity on the adsorption mechanism of dissolved aromatics on activated carbon, Carbon N Y 38 (2000) 1807–1819.
[53] P. Parthasarathy, H.R. Mackey, S. Mariyam, et al., Char products from bamboo waste pyrolysis and acid activation, Front Mater. 7 (2021) 482.
[54] S.S. Sahoo, V.K. Vijay, R. Chandra, H. Kumar, Production and characterization of biochar produced from slow pyrolysis of pigeon pea stalk and bamboo, Clean. Eng. Technol. 3 (2021), 100101.
[55] F. Masís-Meléndez, D. Segura-Chavarría, C.A. García-González, et al., Variability of physical and chemical properties of TLUD stove derived biochars, Appl. Sci. 10 (2020) 507, 507 10.